

Spectroscopy and intruder configurations of ^{33}Mg and ^{31}Ne studied with antisymmetrized molecular dynamics

M. Kimura

Creative Research Institution (CRIS),

Hokkaido University, Sapporo 001-0021, Japan

(Dated: December 18, 2018)

Abstract

Excitation spectra and neutron single particle configurations of ^{33}Mg and ^{31}Ne are investigated by using antisymmetrized molecular dynamics combined with generator coordinate method. It is shown that both nuclei have strongly deformed $3/2^-$ ground state with a $3p2h$ configuration. The excitation spectra are qualitatively understood in terms of the Nilsson model and the calculation has shown the coexistence of different intruder configurations within small excitation energy. The calculated one neutron separation energy of ^{31}Ne is rather small ($S_n = 250$ keV) and implies a p -wave one neutron halo with a strongly deformed core.

PACS numbers: Valid PACS appear here

I. INTRODUCTION

The breaking of neutron magic number $N = 20$ that was firstly pointed out from the observation of the anomalous binding energy and spin of ^{31}Na [1, 2] has been one of the great interests in nuclear physics. Based on the theoretical calculations, neighboring nuclei around ^{31}Na was named “island of inversion” [3, 4] because they are dominated by the intruder configuration in which neutrons are promoted into pf -shell across $N = 20$ shell gap due to strong deformation [5, 6]. Since then, numerous experimental and theoretical studies have been devoted to the island. One of the recent experimental finding is that there are coexistence of “spherical and deformed shape” or “normal and intruder configurations” in many cases [7–10]. It is expected that the exploration of the coexistence will bring us further understanding of the shell structure in neutron rich $N \sim 20$ region.

The spectroscopy of odd-neutron nuclei is of importance and interest, because their spin and parity are related to the last neutron particle’s or hole’s orbit. For example, we have predicted the coexistence of many-particle and many-hole configurations at small excitation energy in ^{31}Mg ($N = 19$) [11], and some of these excited states are identified by the the proton knock-out reaction from ^{32}Al [12]. The spin-parity of the excited states are associated with the neutron orbits $[N, n_z, l_z, j_z] = [2, 0, 2, 3/2], [3, 3, 0, 1/2], [2, 0, 0, 1/2]$ and $[3, 2, 1, 3/2]$ in terms of the Nilsson model.

In this paper, we extend our study to $N = 21$ system (^{33}Mg and ^{31}Ne). Both of them do not have the definite spin-parity assignment for the ground states and information of their excitation spectra is deficient. In the case of ^{33}Mg , there are two major spin-parity assignments of the ground state, $3/2^+$ and $3/2^-$. From the observation of the β decays of ^{33}Na [13] and ^{33}Mg [14], $3/2^+$ assignment is suggested. On the other hand, the measurement of the magnetic moment [15] and one neutron knock-out reaction from ^{34}Mg [16] suggest $3/2^-$. ^{31}Ne is more interesting. Its large reaction cross section [17] and one neutron Coulomb breakup cross section [18] are reported. From the analysis of the one neutron breakup, the assignments of $1/2^+$ or more likely $3/2^-$ are suggested. In both assignments, observed large Coulomb breakup cross section strongly suggests one neutron-halo structure of ^{31}Ne that is firstly observed in the island.

We have applied antisymmetrized molecular dynamics (AMD) with Gogny D1S force [19] to investigate the spectra of ^{33}Mg and ^{31}Ne . It will be shown that both nuclei have

the strongly deformed $3/2^-$ ground states with a neutron $3p2h$ configuration. Similar to $N = 19$ system, different particle-hole configurations coexist within small excitation energy and their spin-parity are associated with the Nilsson-like orbits occupied by the last neutron. It is also shown that the one neutron separation energy of ^{31}Ne is rather small and p -shell neutron-halo structure is possibly formed.

This paper is organized as follows. In the next section, the framework of AMD and the calculational procedure are explained. In the section III, the results are presented. The change of neutron particle-hole configurations as function of deformation is discussed. They are related to the spin-parity of the excitation spectra. The calculated spectra and transition probabilities are compared with the observations, and a theoretical assignment of the excitation spectra is suggested. The final section summarizes this work.

II. THEORETICAL FRAMEWORK

The applied theoretical method is the same as our previous work [11]. The deformed-basis AMD [20, 21] is combined with the generator coordinate method (GCM) to calculate the excitation spectra of $N = 21$ system. The particle-hole configuration is investigated by the analysis of neutron single particle orbits.

A. Wave function, Hamiltonian and variation

The intrinsic wave function of the system with mass A is given by a Slater determinant of single particle wave packets,

$$\Phi_{int} = \mathcal{A}\{\varphi_1, \varphi_2, \dots, \varphi_A\}, \quad \varphi_i(\mathbf{r}) = \phi_i(\mathbf{r})\chi_i\xi_i, \quad (1)$$

where φ_i is the i th single particle wave packet consisting of the spatial ϕ_i , spin χ_i and isospin ξ_i parts. The local Gaussian located at \mathbf{Z}_i is employed as ϕ_i ,

$$\begin{aligned} \phi_i(\mathbf{r}) &= \exp\left\{-\sum_{\sigma=x,y,z} \nu_\sigma \left(r_\sigma - \frac{Z_{i\sigma}}{\sqrt{\nu_\sigma}}\right)^2\right\}, \\ \chi_i &= \alpha_i\chi_\uparrow + \beta_i\chi_\downarrow, \quad |\alpha_i|^2 + |\beta_i|^2 = 1, \\ \xi_i &= \text{proton or neutron.} \end{aligned} \quad (2)$$

Here \mathbf{Z}_i , α_i , β_i and ν_σ are the variational parameters. The parity projected wave function, $\Phi^\pi = \hat{P}^\pi\Phi_{int}$ is the variational wave function.

The Gogny D1S force is employed as an effective nuclear force and the Coulomb force is approximated by a sum of seven Gaussians.

In the present work, we have performed the variational calculation with the constraint on the matter quadrupole deformation β . Variational parameters are optimized by the frictional cooling method so that the energy of the system is minimized for a given constraint on β . The optimized wave function are denoted as $\Phi_{int}(\beta)$. It is noted that we do not put any constraint on the matter quadrupole deformation γ . Therefore γ has the optimal value for each β .

B. Analysis of the single particle orbit

To identify the particle-hole configuration, we analyze the neutron single particle orbital of $\Phi_{int}(\beta)$. We transform the single particle wave packet φ_i to the orthonormalized basis, $\tilde{\varphi}_\alpha = \frac{1}{\sqrt{\lambda_\alpha}} \sum_{i=1}^A c_{i\alpha} \varphi_i$. Here, λ_α and $c_{i\alpha}$ are the eigenvalues and eigenvectors of the overlap matrix $B_{ij} = \langle \varphi_i | \varphi_j \rangle$. Using this basis, the Hartree-Fock single particle Hamiltonian,

$$\begin{aligned}
 h_{\alpha\beta} = & \langle \tilde{\varphi}_\alpha | \hat{t} | \tilde{\varphi}_\beta \rangle + \sum_{\gamma=1}^A \langle \tilde{\varphi}_\alpha \tilde{\varphi}_\gamma | \hat{v}_n + \hat{v}_c | \tilde{\varphi}_\beta \tilde{\varphi}_\gamma - \tilde{\varphi}_\gamma \tilde{\varphi}_\beta \rangle, \\
 & + \frac{1}{2} \sum_{\gamma,\delta=1}^A \langle \tilde{\varphi}_\gamma \tilde{\varphi}_\delta | \tilde{\varphi}_\alpha^* \tilde{\varphi}_\beta \frac{\partial \hat{v}_n}{\partial \rho} | \tilde{\varphi}_\gamma \tilde{\varphi}_\delta - \tilde{\varphi}_\delta \tilde{\varphi}_\gamma \rangle,
 \end{aligned} \tag{3}$$

is defined. The eigenvalues ϵ_s and eigenvectors $f_{\alpha s}$ of $h_{\alpha\beta}$ give the single particle energies and the single particle orbits, $\tilde{\phi}_s = \sum_{\alpha=1}^A f_{\alpha s} \tilde{\varphi}_\alpha$. This procedure gives us information of the occupied neutron orbits. In this paper the particle-hole configuration is denoted as $mpnh$ where m and n respectively denote number of neutron particles in pf -shell and holes in sd -shell in the spherical limit. For example, the normal configuration of $N = 21$ system is denoted as $1p0h$. However, it is noted that this procedure only gives a rough estimation of the particle-hole configuration and should be regarded as a guide to understand the dominant particle-hole configuration of each states. The actual variational wave function is $\Phi^\pi(\beta)$ that is a sum of two Slater determinant. And we then perform the angular momentum projection and GCM calculation that superpose thousands of Slater determinants. Therefore our final wave function explained in the next subsection is beyond a simple single particle picture.

C. Angular momentum projection and GCM

After the variational calculation, we project out an eigenstate of the total angular momentum J ,

$$\Phi_{MK}^{J\pm}(\beta) = \hat{P}_{MK}^J \Phi^\pm(\beta) \quad (4)$$

Here \hat{P}_{MK}^J is the total angular momentum projector. The integrals over three Euler angles are evaluated by the numerical integration. The calculation is completed by performing GCM. The wave functions $\Phi_{MK}^{J\pm}(\beta)$ which have the same parity and angular momentum but have different K , deformation β and single particle configurations are superposed. Then the wave function of the system is expressed as

$$\Phi_n^{J\pm} = c_n \Phi_{MK}^{J\pm}(\beta) + c'_n \Phi_{MK'}^{J\pm}(\beta') + \dots, \quad (5)$$

where the quantum numbers except for the total angular momentum and the parity are represented by n . The coefficients c_n, c'_n, \dots are determined by the Hill-Wheeler equation. The physical quantities discussed in the next section are basically calculated from the GCM wave function, Eq. (5).

III. RESULTS AND DISCUSSIONS

A. Energy curve and single particle configurations of ^{33}Mg

Energy curves obtained by the variational calculation after the parity projection are presented in Fig. 1 (a) and (b) with circles. For a given value of β , there is sometimes a local minimum solution together with the global minimum. In such case, both minima are plotted for the same value of β . For any value of β , ^{33}Mg preferred prolate deformation ($\gamma > 30^\circ$) over oblate deformation ($\gamma < 30^\circ$). The positive-parity states have two minima and they have neutron $2p1h$ and $4p3h$ configurations in the ascending order of deformation. The negative-parity states have three minima with $1p0h$, $3p2h$ and $5p4h$ configurations. The particle-hole configurations of those minima are confirmed by the analysis of the neutron single particle orbits. Figure 1 (c) and (d) shows the single particle energies of the last 7 neutrons as function of deformation. In the case of the negative parity, the last neutron occupies $f_{7/2}$ orbit and other neutrons fill sd -shell at small deformation. Therefore, the

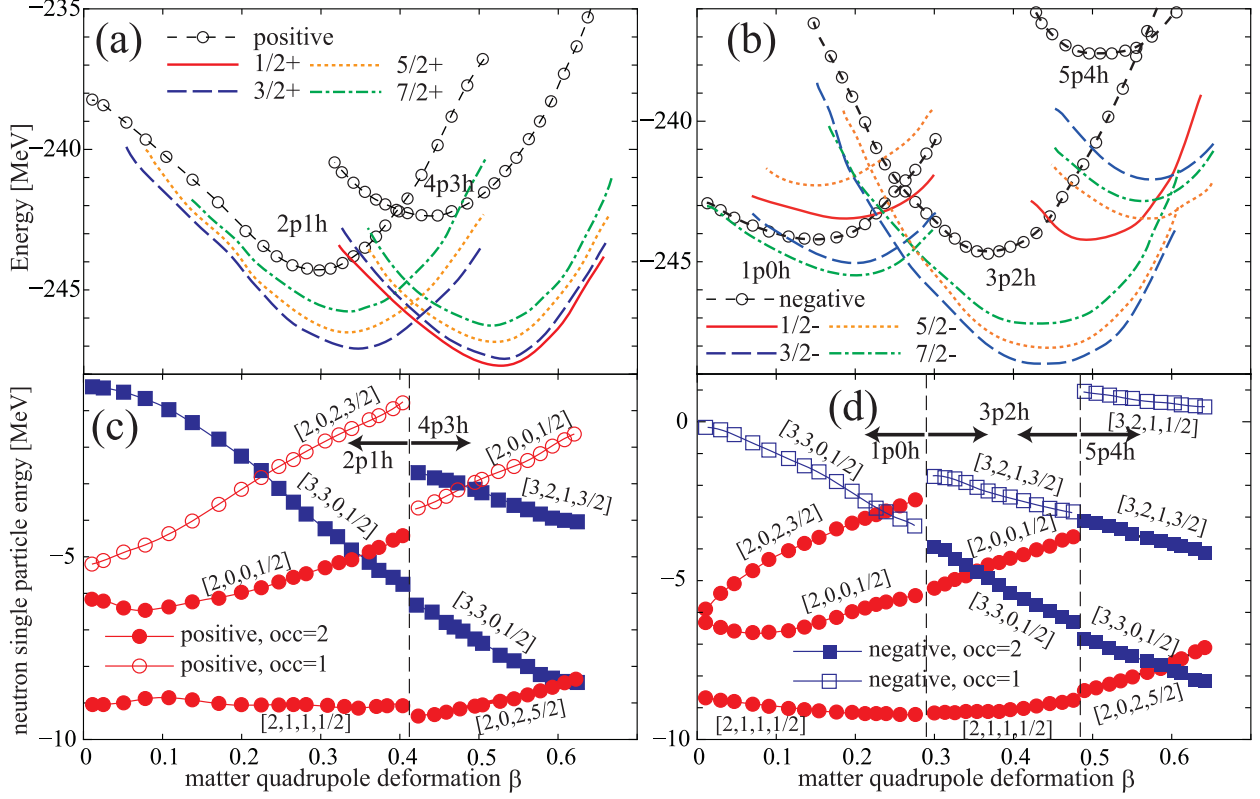


FIG. 1: (color online) (a) and (b): Energy curves of ^{33}Mg before and after angular momentum projection for (a) positive- and (b) negative-parity states. Circles with dashed lines show the energy curve before the angular momentum projection. Colored lines show the energy curves after the angular momentum projection to $J = 1/2, 3/2, 5/2$ and $7/2$. (c) and (d): Corresponding single particle energies of the last 7 neutrons. Filled (open) symbols show the orbits occupied by two (one) neutrons. Circles (boxes) show the orbits in which positive-parity (negative-parity) component is larger than 50 %.

minimum around $\beta = 0.2$ in Fig. 1 (b) has a neutron $1p0h$ configuration. As deformation becomes larger, neutron single particle energies show Nilsson model like behavior. Two orbits originate in $f_{7/2}$ come down and $d_{3/2}$ splits into two orbits and go up. They are respectively denoted as $[N, n_z, l_z, j_z] = [3, 3, 0, 1/2], [3, 2, 1, 3/2], [2, 0, 2, 3/2]$ and $[2, 0, 0, 1/2]$ in terms of Nilsson model. Around $\beta = 0.25$ the configuration changes. Two neutrons occupy $[3, 3, 0, 1/2]$ and one occupies $[3, 2, 1, 3/2]$ orbit. The $[2, 0, 2, 3/2]$ orbit is now empty. Thus the second minimum of the energy curve has a $3p2h$ configuration. Further increase of deformation pulls down the $[3, 2, 1, 1/2]$ orbit originates in $p_{3/2}$. The last neutron occupies it and two orbits originate in $d_{3/2}$ become empty. Therefore third minimum that appears

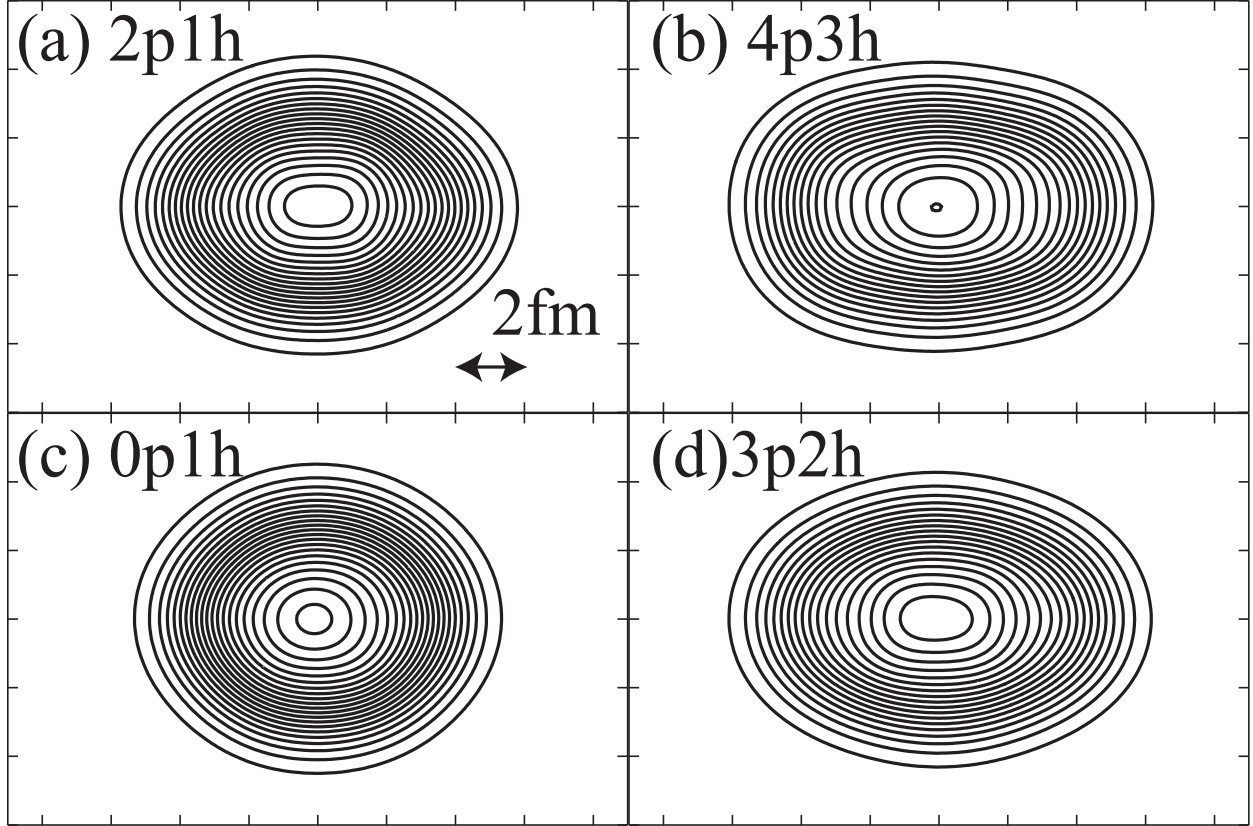


FIG. 2: Intrinsic density distributions at minima of energy curves. (a) and (b) show the minima of positive-parity states. (c) and (d) show $0p1h$ and $3p2h$ minima of negative-parity states.

as the local minimum above the $3p2h$ configuration has a $5p4h$ configuration. Its energy is rather higher than other two configurations. The positive-parity curve is also understood in the same way. It has two minima that have respectively $2p1h$ and $4p3h$ configurations. The corresponding intrinsic matter density distributions are shown in Fig. 2. It shows an almost spherical shape of the normal configuration ($1p0h$) and deformation becomes larger as number of neutrons in pf -shell increases.

The energy curves and corresponding neutron single particle orbits show the qualitative agreement with the Nilsson model picture discussed in Ref. [22, 23]. The neutron single particle orbits split and change their order depending on deformation of the system. As deformation becomes larger, number of particle in the orbits originate in pf -shell increases. However, it is reminded that the analysis of the neutron single particle orbits gives only a rough estimation of the particle-hole configuration. Indeed, there are strong parity mixing of the neutron single particle orbits. For example, the orbit denoted as $[3,2,1,1/2]$ in Fig. 1 (d)

has the strongest parity mixing where the the positive-parity component amounts to about 40%. The parity mixing becomes stronger as deformation larger. This may mean that the strongly deformed states have a complicated mixing of different particle-hole configurations and are beyond the Nilsson model picture.

Adding to the Nilsson model like behavior, the present calculation has shown the following two points. (1) ^{33}Mg is strongly deformed and quite soft against deformation. The intruder $3p2h$ configuration is already the lowest energy configuration at this stage and other particle-hole configurations also appear within very small excitation energy. (2) The last neutron walks around the $[3,3,0,1/2]$, $[2,0,2,3/2]$, $[3,2,1,3/2]$, $[2,0,0,1/2]$ and $[3,2,1,1/2]$ orbits as deformation becomes larger. These neutron orbits will characterize the spin-parity of the corresponding excited states or rotational bands.

Lines in Fig. 1 show the energy curves after the angular momentum projection. The energies of strongly deformed states are lowered by more than 5 MeV. The lowest energy state at this stage is the $3/2^-$ state with the $3p2h$ configuration. More importantly, the property of the last neutron orbital is reflected to the excitation spectrum of each configuration. Deformation of $1p0h$ configuration is the smallest among all minima and it generates low-lying $7/2^-$ and $3/2^-$ states that are respectively attributed to the almost spherical neutron $f_{7/2}$ and $p_{3/2}$ orbits. In the case of other minima, rotational spectra appear depending on the last neutron orbit. For example, the $3p2h$ configuration has the last neutron in the $[3,2,1,3/2]$ orbit and it generates the $K^\pi = 3/2^-$ rotational spectrum. In the same way, the $2p1h$, $4p3h$ and $5p3h$ configurations respectively generate the $K^\pi = 3/2^+$, $1/2^+$ and $1/2^-$ spectra that are associated with the asymptotic quantum number j_z of the last neutron.

B. Spectrum of ^{33}Mg and transitions

Figure. 3 shows the low-lying spectrum of ^{33}Mg obtained by GCM. Tentative assignments given in Refs. [13, 15] are also shown. The calculated binding energy of ^{33}Mg is 251.1 MeV that underestimates the observed value by about 1 MeV. The one neutron separation energy is 1.9 MeV that is not far from the observed value (2.22 MeV). The ground state is the $3/2^-_1$ state and dominated by the $3p2h$ configuration that approximately amounts to 87%. Here the amount of the $3p2h$ configuration in the ground state is estimated by calculating the overlap between the ground state GCM wave function ($\Phi_{g.s.}^{3/2^-}$) and the wave function of $3/2^-$

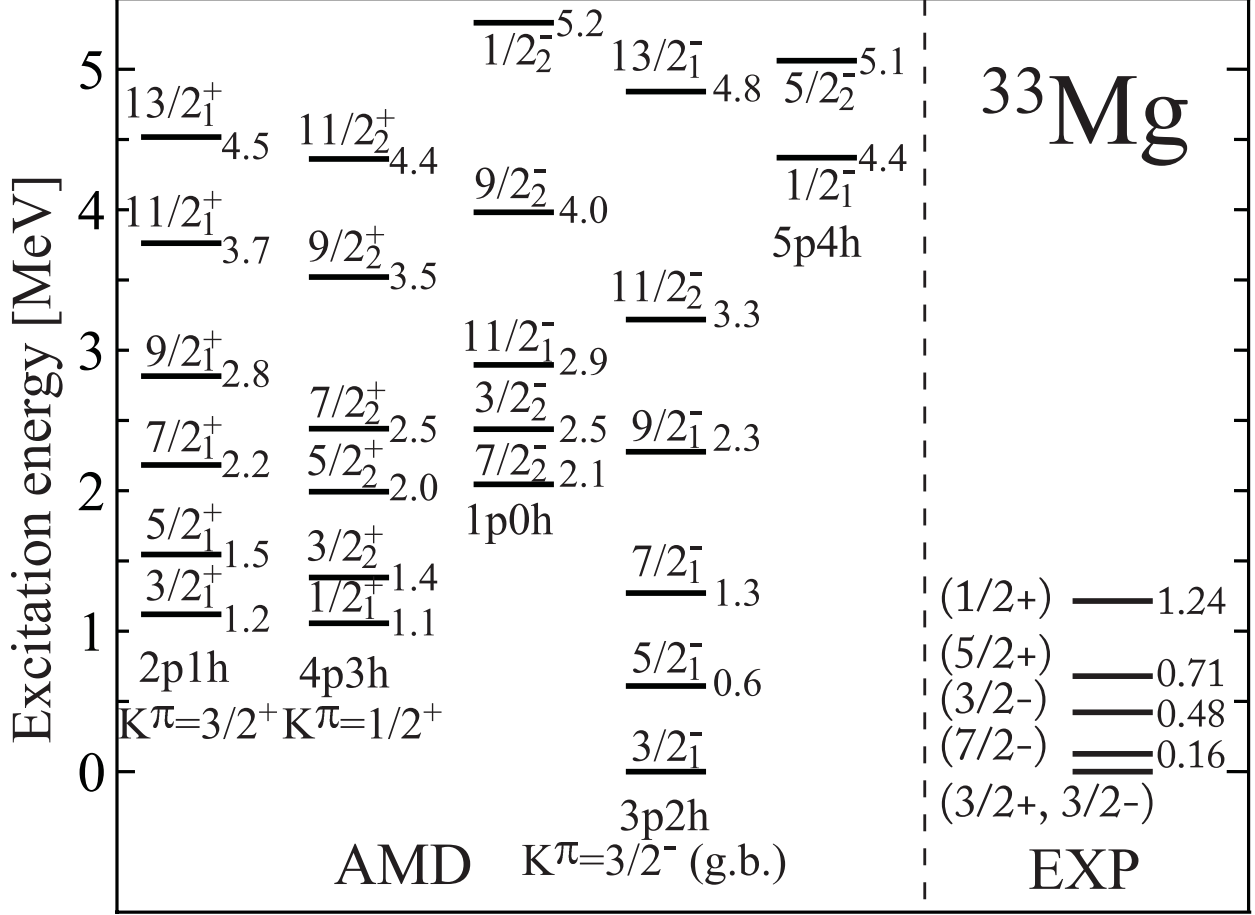


FIG. 3: Calculated spectrum of ^{33}Mg compared with the tentative assignments suggested in Refs. [13, 15]. $mpnh$ configurations shown below each bands mean the dominant particle configuration. Numbers show excitation energies in MeV.

minimum ($\Phi^{3/2^-}(\beta = 0.45)$) in Fig. 1 (b),

$$|\langle \Phi_{g.s.}^{3/2^-} | \Phi^{3/2^-}(\beta = 0.45) \rangle|^2. \quad (6)$$

The $3p2h$ configuration dominates the ground band $K^\pi = 3/2^-$ that has the first excited state $5/2_1^-$ at 0.6 MeV. The normal configuration $1p0h$ is located at higher excitation energy. The $7/2_2^-$ and $3/2_2^-$ states at 2.1 and 2.5 MeV are understood as the almost spherical $f_{7/2}$ and $p_{3/2}$ single particle states. The $2p1h$ and $3p2h$ configurations appear around 1 MeV. They respectively dominate the $K^\pi = 3/2^+$ and $1/2^+$ rotational bands. Similar to ^{31}Mg , many-particle and many-hole states with different deformation coexist within rather small excitation energy.

The calculated $B(E2)$ values are summarized in Table. I for several low-lying states.

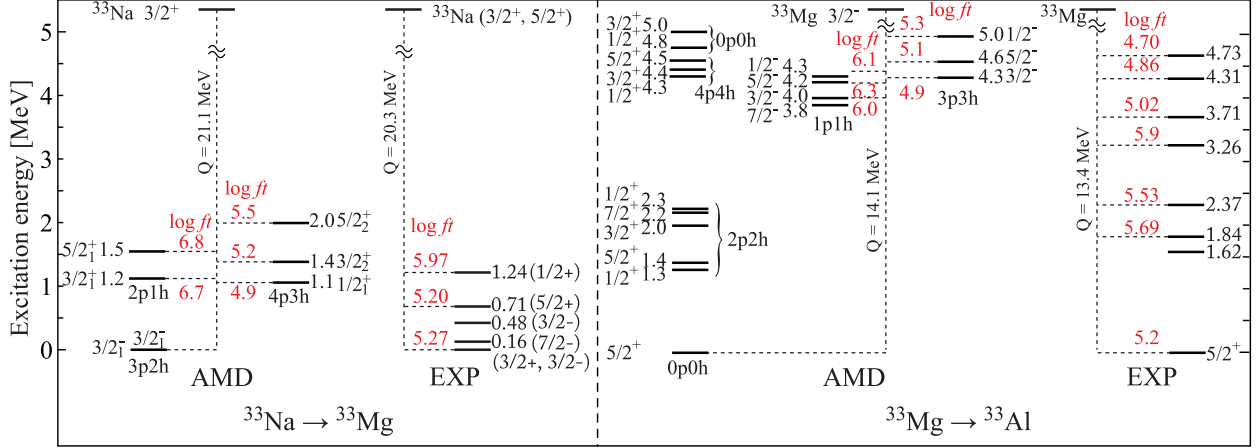


FIG. 4: (color online) Calculated and observed [13, 14] β decay strength of $^{33}\text{Na} \rightarrow ^{33}\text{Mg}$ (left) and $^{33}\text{Mg} \rightarrow ^{33}\text{Al}$ (right).

Except for the $1p0h$ configuration, the intra-band $E2$ transitions are large due to their deformation. Because of the mixing between different particle-hole configurations, there are non negligible inter-band $E2$ transitions between the $K^\pi = 3/2^+$ and $1/2^+$ bands. The β decay strength from ^{33}Na and to ^{33}Al are shown in Fig. 4. The wave functions of ^{33}Na and ^{33}Al are calculated by using the same method as ^{33}Mg . The ground state of ^{33}Na is $3/2^+$ and dominated by a neutron $4p2h$ configuration and mixed with a $2p0h$ configuration (10%) in the present calculation. Therefore the β decay strongly feeds the $4p3h$ configuration of ^{33}Mg . The β decay to ^{33}Al mainly feeds the $3p3h$ configuration, since the ground state of ^{33}Mg is dominated by a $3p2h$ configuration. It feeds the $3/2^-$, $5/2^-$ and $1/2^-$ states around 4.5 MeV strongly.

Then we compare our results with observations and examine the spectrum of ^{33}Mg . Our result supports the $3/2^-$ assignment of the ground state suggested from the magnetic moment and two neutron knock-out reaction. Indeed the calculated $3/2^-_1$ state gives the closest value to the observed magnetic moment among the lowest energy states of particle-hole configurations (Table. II). The calculated first excited state ($5/2^-_1$) at 0.6 MeV may correspond to the observed 0.48 MeV state, because the large Coulomb excitation cross section from the ground state to this state is reported and large quadrupole deformation $\beta_C = 0.52$ is extracted [24]. Experimentally, the first excited state was reported at 0.16 MeV from the β decay measurement of ^{33}Na . Since there was no direct β decay feeding of this state, a tentative assignment of $7/2^-$ was given. In our calculation, there is not

TABLE I: Calculated intra- and inter-band $E2$ transition probabilities in $e^2\text{fm}^4$

band	J_i^π	J_f^π	$B(E2; J_i^\pi \rightarrow J_f^\pi)$
g.b. \rightarrow g.b.	$3/2_1^-$	$5/2_1^-$	282
	$3/2_1^-$	$7/2_1^-$	154
	$5/2_1^-$	$7/2_1^-$	147
	$5/2_1^-$	$9/2_1^-$	194
	$7/2_1^-$	$9/2_1^-$	92
$K^\pi = 1/2^+ \rightarrow 1/2^+$	$1/2_1^+$	$3/2_2^+$	275
	$1/2_1^+$	$5/2_2^+$	426
	$3/2_2^+$	$5/2_2^+$	66
	$3/2_2^+$	$7/2_2^+$	357
	$5/2_2^+$	$7/2_2^+$	24
$K^\pi = 3/2^+ \rightarrow 3/2^+$	$3/2_1^+$	$5/2_1^+$	188
	$3/2_1^+$	$7/2_1^+$	103
	$5/2_1^+$	$7/2_1^+$	99
$1p0h \rightarrow 1p0h$	$7/2_2^-$	$3/2_2^-$	31
	$7/2_2^-$	$11/2_2^-$	23
$K^\pi = 1/2^+ \rightarrow 3/2^+$	$1/2_1^+$	$3/2_1^+$	11
	$1/2_1^+$	$5/2_2^+$	19
	$3/2_2^+$	$5/2_1^+$	18
	$3/2_2^+$	$7/2_1^+$	30

corresponding state with very small excitation energy. The observed 0.71 and 1.24 MeV states could be associated with the calculated $1/2_1^+$ (1.1 MeV) and $3/2_2^+$ (1.4 MeV) states of $K^\pi = 1/2^+$ band from their $\log ft$ values. However, the present calculation does not explain the β decay of ^{33}Na to the ground state of ^{33}Mg nor that of ^{33}Mg to ^{33}Al . Especially, our calculation has no β decay feeding of low-lying states of ^{33}Al below 4 MeV, while there are 5 transitions including the feeding of the ground state of ^{33}Al are reported. To explain those transitions, we need the positive-parity ground state of ^{33}Mg .

An alternative assignment for the ground state of ^{33}Mg could be $1/2_1^+$ with the $4p3h$

TABLE II: Calculated and observed [15] magnetic moments in the unit of μ_N . Theoretical values are shown for the lowest energy states of particle-hole configurations.

	$3/2_1^-(3p2h)$	$7/2_1^-(1p0h)$	$3/2_1^+(2p1h)$	$1/2_1^+(4p3h)$	exp.
μ_N	-0.70	-1.61	0.89	-0.91	-0.7456

configuration, since its magnetic moment has the same sign with and is not far from the observed value. Though the $1/2_1^+$ state is located at 1.1 MeV in the present calculation, a minor modification of the Gogny force parameter might make it the ground state. In this case, the observed β decay data of ^{33}Na could be compatible. The observed 0.71 and 1.24 MeV states could be associated with the $3/2_2^+$ and $5/2_2^+$ states at 1.4 and 2.0 MeV from their $\log ft$ values. Their excitation energies measured from the $1/2_1^+$ state are 0.4 and 1.0 MeV. The observed 0.16 and 0.48 MeV states might be associated with the negative-parity states with $1p0h$ or $3p2h$ configurations. However, even in this scenario, we cannot explain the β decay of ^{33}Mg . The $1/2_1^+$ state with $4p3h$ configuration would strongly feed the states of ^{33}Al dominated by $4p4h$ configuration that are located around 4.4 MeV in the present calculation. These transitions could be associated with the observed strong decays to 3.71, 4.31 and 4.73 MeV states. The problem is that this assignment neither explains the feeding of the states below 4 MeV. There are only the excited states with a $2p2h$ configuration and the ground state with the $0p0h$ configurations below 4 MeV. Since there is always the mixing between different particle-hole configuration, the $1/2_1^+$ ground state of ^{33}Mg could feed these states, but it will never explain the strong feeding of the ground state of ^{33}Al that is dominated by $0p0h$ configuration.

Thus the present calculation partially explains some of observations but is incompatible with some in any interpretation. Further detailed study including the spectra of ^{33}Na and ^{33}Al is required to settle down this problem, that will be done in near future.

C. Spectrum of ^{31}Ne

Since neutron number is the same, the energy curves and particle-hole configurations of ^{31}Ne are qualitatively similar to ^{33}Mg . The difference is in the relative energies between particle-hole configurations. The calculated energy spectrum is shown in Fig. 5. The

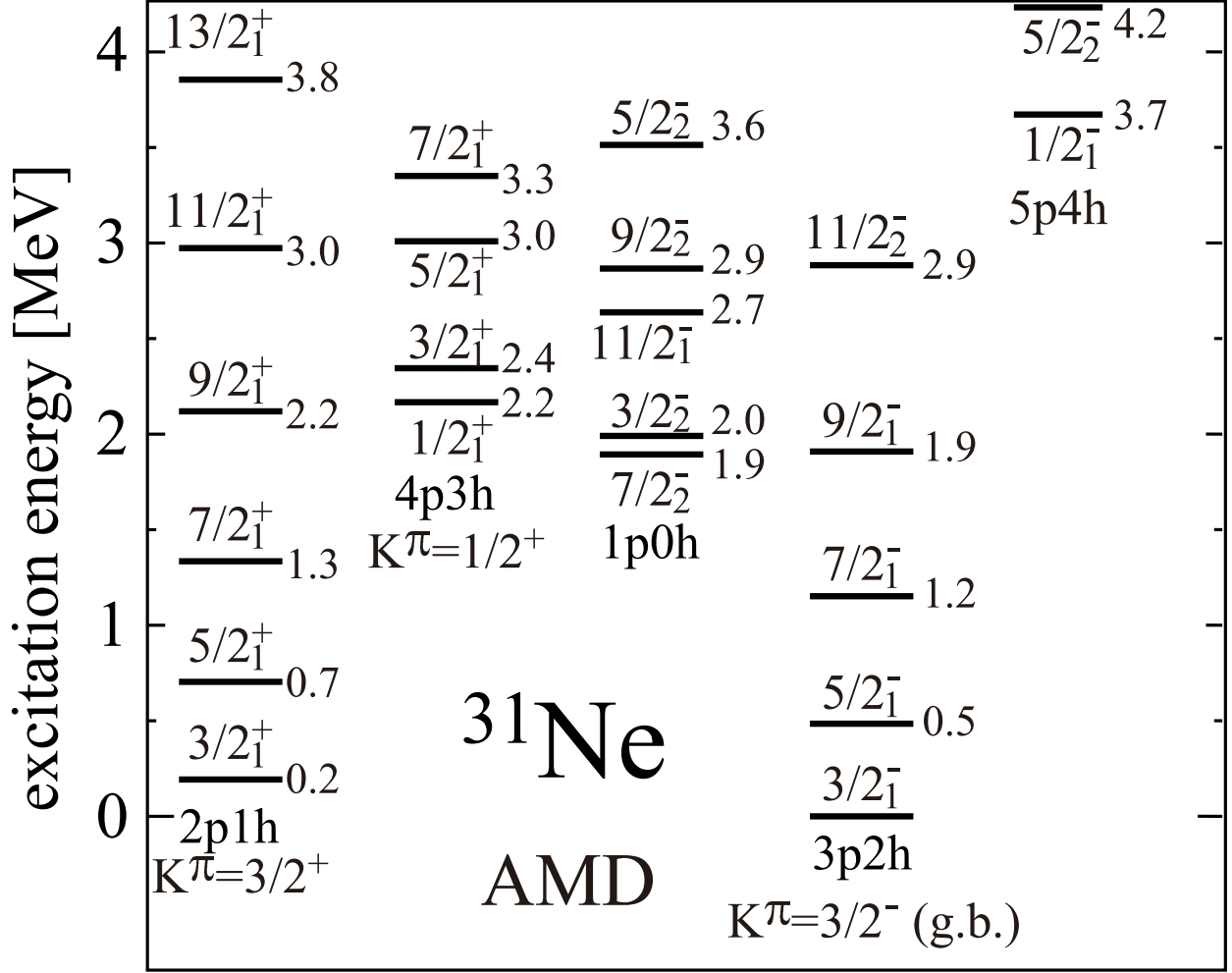


FIG. 5: Calculated spectrum of ^{31}Ne . $mpnh$ configurations shown below each bands mean the dominant particle configuration. Numbers show excitation energies in MeV.

ground state is the $3/2_1^-$ state dominated by the $3p2h$ configuration. Different from ^{33}Mg , the $K^\pi = 3/2^+$ band ($2p1h$) is located at smaller excitation energy and the $K^\pi = 1/2^+$ band is at higher excitation energy. We conjecture that their excitation energies are sensitive to the neutron excess, since we have found a minor modification of the isospin dependence of Gogny force strongly affects their energies.

Experimentally, small one neutron separation energy $S_n = 0.29 \pm 1.64$ MeV is reported [25]. But neither the ground state spin-parity nor excitation spectrum are not well established. The assignment of ground state $3/2^-$ or $1/2^+$ is suggested from the Coulomb breakup reaction [18]. From these observations, the p -wave or s -wave neutron halo structure is suggested and theoretically investigated [26]. Therefore, we focus on the ground state property

of ^{31}Ne . The calculated one neutron separation energy is $S_n = 250$ keV that is fairly smaller than ^{33}Mg . Combined with the calculated ground spin-parity of $3/2^-$, ^{31}Ne is a promising candidate of a p -wave halo nucleus as suggested in Ref. [18]. The ground state of ^{31}Ne can be approximately regarded as the two body system consists of a ^{30}Ne core with $2p2h$ configuration and a neutron in $[3,2,1,3/2]$ orbit. Since the ground band of ^{30}Ne is dominated by $2p2h$ configuration [27, 28], there should be the collective excitation of ^{30}Ne core in ^{31}Ne . The calculated matter root mean square radius of ^{31}Ne is 3.42 fm that is larger than ^{30}Ne (3.31 fm), ^{32}Ne (3.40 fm) and ^{33}Mg (3.34 fm). However, the neutron density distribution does not have a halo-like tail. This is due to the limitation of the present calculation. Since the single particle wave function is limited to the Gaussian form, it cannot describe a halo tail. Improvement of the neutron wave function by combining the AMD with the resonating group method will be made in our next study.

IV. SUMMARY

In summary, we have studied the spectra of ^{33}Mg and ^{31}Ne . Both nuclei have the strongly deformed $3/2^-$ ground state with a $3p2h$ configuration and the coexistence of many different particle-hole configurations within small excitation energy. Their spectra are qualitatively understood in terms of the Nilsson model. The last neutron occupies $[N, n_z, l_z, j_z] = [3, 3, 0, 1/2]$, $[2, 0, 2, 3/2]$, $[3, 2, 1, 3/2]$, $[2, 0, 0, 1/2]$ and $[3, 2, 1, 1/2]$ depending on deformation of the system and the corresponding excited states or rotational bands are formed. The calculated spectrum of ^{33}Mg is examined based on the comparison with the observed magnetic moment and β decays. The $3/2^-$ assignment for the ground state by the present calculation agrees with the observed magnetic moment, but does not explain the β decays. An alternative assignment of $1/2^+$ is also examined, but not compatible with the observed $^{33}\text{Mg} \rightarrow ^{33}\text{Al}$ (g.s.) decay. This requires further detailed study of the $A = 33$ isobars. ^{31}Ne also has the $3/2^-$ ground state. The calculated small one neutron separation energy (250 keV) supports the p -wave neutron halo structure.

[1] C. Thibault *et al.*, Phys. Rev. C **12**, 644 (1975).

[2] G. Huber *et al.*, Phys. Rev. C **18**, 2342 (1978).

- [3] A. Poves and J. Retamosa, *Phys. Lett. B* **184**, 311 (1986).
- [4] E. K. Warburton, J. A. Becker and B. A. Brown, *Phys. Rev. C* **41**, 1147 (1990).
- [5] N. Fukunishi, T. Otsuka and T. Sebe, *Phys. Lett. B* **296**, 279 (1992).
- [6] T. Motobayashi *et al.*, *Phys. Lett. B* **346**, 9 (1995).
- [7] S. Takeuchi *et al.*, *Phys. Rev. C* **79**, 054319 (2009).
- [8] W. Schwerdtfeger *et al.*, *Phys. Rev. Lett.* **103**, 012501 (2009).
- [9] Z. M. Wang *et al.*, *Phys. Rev. C* **81**, 064301 (2010).
- [10] K. Wimmer *et al.*, *Phys. Rev. Lett.* **105**, 252501 (2010).
- [11] M. Kimura, *Phys. Rev. C* **75**, 041302 (2007).
- [12] D. Miller *et al.*, *Phys. Rev. C* **79**, 054306 (2009).
- [13] S. Nummela *et al.*, *Phys. Rev. C* **64**, 054313 (2001).
- [14] V. Tripathi *et al.*, *Phys. Rev. Lett.* **101**, 142504 (2008).
- [15] D. T. Yordanov *et al.*, *Phys. Rev. Lett.* **99**, 212501 (2007).
- [16] R. Kanungo *et al.*, *Phys. Lett. B* **685**, 253 (2010).
- [17] M. Takechi *et al.*, *Nucl. Phys. A* **834**, 412c (2010).
- [18] T. Nakamura *et al.*, *Phys. Rev. Lett.* **103**, 262501 (2010).
- [19] J. Dechargé and D. Gogny, *Phys. Rev. C* **21**, 1568 (1980).
- [20] M. Kimura, Y. Sugawa and H. Horiuchi, *Prog. Theor. Phys. (Kyoto)* **106**, 1153 (2001).
- [21] M. Kimura, *Phys. Rev. C* **69**, 044319 (2004).
- [22] I. Hamamoto, *Phys. Rev. C* **76**, 054319 (2007)
- [23] I. Hamamoto, *Phys. Rev. C* **81**, 021304(R) (2010).
- [24] B. V. Pritychenko *et al.*, *Phys. Rev. C* **65**, 061304(R) (2002).
- [25] B. Jurado *et al.*, *Phys. Lett. B* **649**, 43 (2007).
- [26] W. Horiuchi, Y. Suzuki, P. Capel and D. Baye, *Phys. Rev. C* **81**, 024606 (2010).
- [27] M. Kimura and H. Horiuchi, *Prog. Theor. Phys. (Kyoto)* **107**, 33 (2002).
- [28] M. Kimura and H. Horiuchi, *Prog. Theor. Phys. (Kyoto)* **111**, 841 (2004).